Backbone and side-chain proton NMR assignment in fully protonated proteins: microcrystals, sedimented assemblies, and amyloid fibrils

Jan Stanek,[a] Loren B. Andreas,[a] Kristaps Jaudzems,[a] Diane Cala,[a] Daniela Lalli,[a] Andrea Bertarello,[a] Tobias Schubeis,[a] Inara Akopjana,[b] Svetlana Kotelovica,[b] Kaspars Tars,[b] Andrea Pica,[c] Serena Leone,[c] Delia Picone,[c] Zhi-Qiang Xu,[d] Nicholas E. Dixon,[d] Denis Martinez,[e] Mélanie Berbon,[e] Nadia El Mammeri,[e] Abdelmajid Noubhani,[e] Sven Saupe,[f] Birgit Habenstein,[e] Antoine Loquet,[e] and Guido Pintacuda[a*]

[a] *Centre de RMN à Très Hauts Champs, Institut des Sciences Analytiques (UMR 5280 - CNRS, ENS Lyon, UCB Lyon 1), Université de Lyon, 69100 Villeurbanne, France*
[b] *Biomedical Research and Study Centre, Riga, Latvia*
[c] *Department of Chemical Sciences, University of Naples Federico II, Via Cintia, I-80136, Naples, Italy*
[d] *School of Chemistry, University of Wollongong, NSW 2522, Australia*
[e] *Institute of Chemistry & Biology of Membranes & Nanoobjects (UMR 5248 CBMN - CNRS, U. Bordeaux, Bordeaux INP), 33600 Pessac, France*
[f] *Institut de Biochimie et de Génétique Cellulaire (UMR 5095, CNRS - Université de Bordeaux), 33077 Bordeaux, France*

SUPPORTING INFORMATION

I. SAMPLE PREPARATION

GB1. Uniformly ^{13}C,^{15}N-labeled GB1 with the T2Q mutation was purchased from Giotto Biotech (Sesto Fiorentino, Italy). The sample was dialyzed extensively against phosphate buffer. The concentration was increased to about 25 mg per mL using a 3 kD Amicon concentrator (EMD Millipore, Darmstadt, Germany) and micro-crystallized by serial addition (an equal volume to the protein solution was added 3 times) of a mixture of methyl-2-4-pentane-diol and isopropanol according to a previously described protocol.[1]

AP205CP. Uniformly ^{13}C,^{15}N-labeled AP205 coat protein[2] was expressed in *E. coli* using a modified pETDuet vector (Novagen). Bacteria were grown in 100% H_2O medium enriched with ^{13}C-glucose (2 g/L) and ^{15}N-labeled ammonium chloride (1 g/L) until they reached OD_{600}=0.7. IPTG was added to 1 mM final concentration and cells were grown for 4 more hours before being centrifuged and frozen. Lysis buffer (40 mM tris-HCl, pH 8.0, 300 mM NaCl, 1 mg/ml lysozyme, 10 μg/ml DNase, 10 mM $MgCl_2$,) was added (3 mL per gram of cells), and cells were further lysed by sonication. The resulting solution was centrifuged, and the supernatant was loaded on a sepharose CL-4B (GE Healthcare) column. The resulting fractions containing the capsids were further purified on a Fractogel (Merck) ion-exchange column. The eluent was concentrated to 10 mg/mL using a 10 kD Amicon concentrator and crystallized in hanging drops by addition of an equal volume of precipitant solution (10 mM HEPES pH 7.5, 0.1M NaCl and 10% PEG w/v 4000).
Microcrystals were harvested and packed by ultracentrifugation at 165,000×*g* for 15 h at 12°C directly into the NMR rotor using a device provided by Giotto Biotech, similar to those described in literature.[3,4]
Note that the signal of polyethylene glycol (PEG) resonating at the edge of the Hα region can be of concern for the proteins such as AP205, which utilize it for crystallization. In those cases the most straightforward solution is to use a perdeuterated PEG (Polymer Source, Dorval, QC Canada).

HET-s. Uniformly ^{13}C,^{15}N-labeled HET-s(218-289) was expressed, purified and assembled as previously described.[5]

MNEI. Uniformly labeled ^{13}C,^{15}N-MNEI was produced in *Escherichia coli* BL21(DE3) freshly transformed with the pET22b+_MNEI vector.[6] Cells were cultured in 1 L of M9 medium supplemented with 100 mg/L ampicillin, 4 g/L ^{13}C-glucose, 5g/L $^{15}NH_4Cl$ and trace elements. Protein expression was induced at OD_{600} = 0.8 with 0.4 mM IPTG at 37°C for 5 h. Purification was achieved with a one-step procedure as described.[7] Protein yield was estimated by UV absorbance and was on average 20 mg per liter of culture. After lyophilization, the protein was dissolved in 20 mM sodium phosphate pH 2.5 at a concentration of 10 mg/mL and crystallized in hanging drops by addition of an equal volume of precipitant solution (0.1 M sodium acetate pH 5.0, 0.2 M ammonium sulphate, and 25% (w/v) PEG 4000). Microcrystals were harvested and packed by ultracentrifugation at 150,000×*g* for 12 h at 4°C directly into the 0.7mm NMR rotor using a device provided by Giotto Biotech.[3,4]

β_2 sliding clamp. The β_2 sliding clamp was overproduced in *E. coli* BL21(lDE3)*recA* containing plasmid pND261.[8] Cells were grown in 2 L of M9 minimal medium containing 1 g/L ^{15}N-NH_4Cl and 1 g/L ^{13}C-glucose at 30˚C (until they reached OD_{600}=0.6), and protein production was induced over 4 h at 42˚C. β_2 was purified as described,[8] concentrated using a Vivaspin-2 10kDa-cutoff centrifugal concentrator to 30 mg/mL in a buffer containing 50mM Tris (pH 7.6), 1 mM DTT and 0.5 mM EDTA, and sedimented into a 0.7mm MAS rotor at 150000×*g* at 4˚C over 62 h.

II. ^{15}N-^{1}H CORRELATIONS

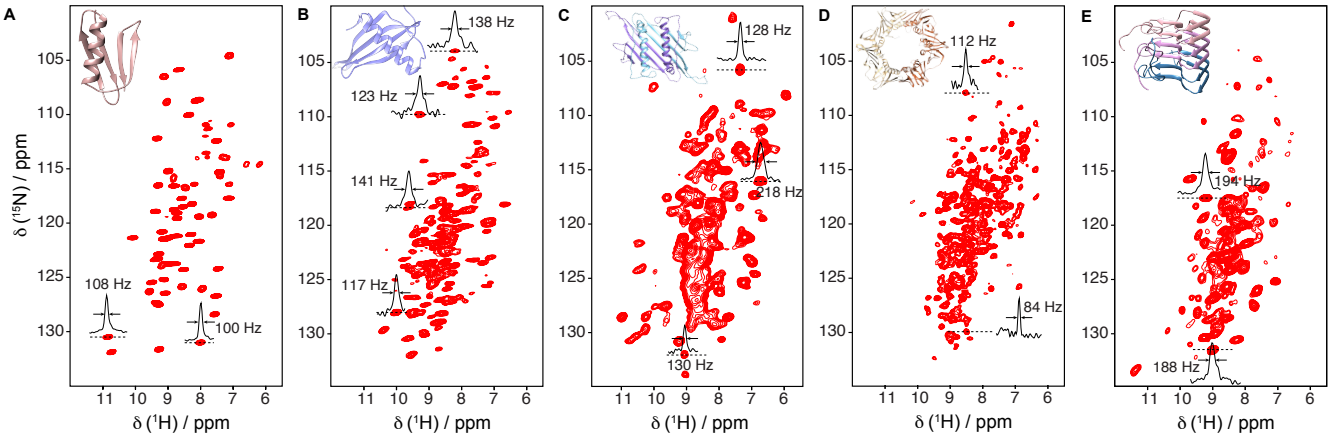

Figure S1. ^{15}N-^{1}H CP-HSQC spectra of GB1 (A), MNEI (B), AP205 coat protein (C), β_2 sliding clamp (D) and HET-s (E), acquired at the 1 GHz (GB1, AP205, β_2 clamp, HET-s) and 800 MHz (MNEI) spectrometers and MAS rate of 111 kHz (GB1, MNEI, β_2 clamp) or 100 kHz (AP205, HET-s). 1D traces with representative ^{1}H line widths are provided for isolated peaks.

III. ^{1}H LINEWIDTHS

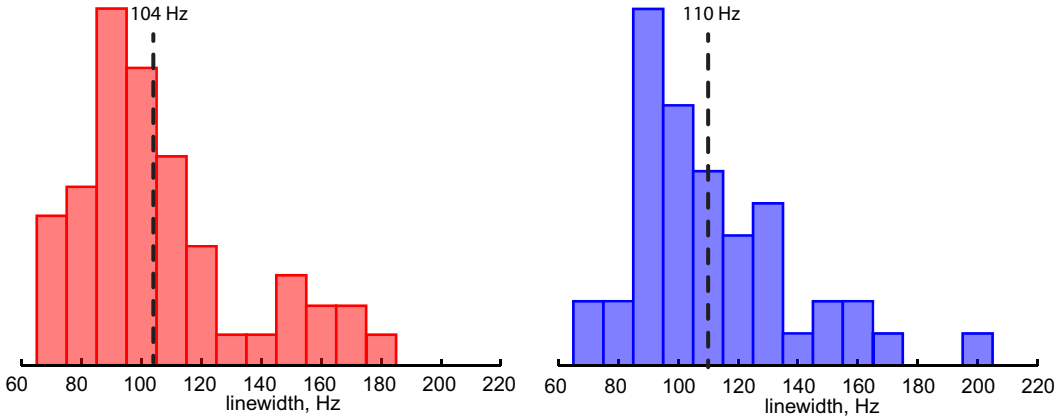

Figure S2. Histograms of ^{1}H line widths of 54 and 45 isolated peaks in ^{13}C- (in *red*) and ^{15}N-CP-HSQC (in *blue*) of GB1. No window function was employed, and ^{1}H signal was truncated to 13 ms. The median of obtained values is shown in each plot.

In the case of GB1 the ^{1}H line widths were approximated by Gaussian line fitting of peaks in the well-resolved 2D ^{13}C and ^{15}N-CP-HSQC spectra. No window function was used for the ^{1}H dimension. As shown in Fig S2, the median of ^{1}H line widths is 110 Hz and 104 for amide and α-protons, respectively. The homogenous contribution to the line width is approximately 68 Hz (estimated as $1/(\pi T_2')$). T2′ was measured from a series of 1D spin-echo spectra by integrating over all proton resonances. Assuming that $(lw)^2=(lw_{\text{inhom}})^2+(lw_{\text{hom}})^2$, we estimate the inhomogeneous contribution to be 86 Hz and 79 Hz for $^{1}H^{N}$ and $^{1}H\alpha$, respectively.

For the HET-s sample (at the MAS rate of 100 kHz), the line widths of amide ^{1}H and ^{15}N were estimated as full width at the half-height (without fitting) on a subset of 16 isolated peaks in the ^{15}N-CP-HSQC spectrum. Amide ^{1}H line widths varied from 124 to 247 Hz with a median of 194 Hz. Homogenous contribution to $^{1}H^{N}$ is 130 Hz, as estimated from the bulk T_2' measurements (2.5 ms). The line widths of $^{1}H\alpha$ were measured in ^{13}C-CP-HSQC for 13 isolated peaks. They varied between 106

and 186 Hz, with a median of 140 Hz. This is less than for amide ^{1}H despite somewhat larger homogeneous contribution to the line width (144 Hz on average), suggesting that amide protons experience larger inhomogeneous broadening, while the ^{1}Hα resonances are primarily homogeneously broadened.

For AP205CP, amide and alpha proton line widths were measured in the same way using 21 and 18 isolated peaks in ^{15}N- and ^{13}C-CP-HSQC spectra. The median of $^{1}H^{N}$ and ^{1}Hα were 174 and 153 Hz, respectively. Similarly to HET-s, the homogenous contribution to the ^{1}H line width was slightly smaller for amide than for alpha protons (106 and 118 Hz, respectively). Thus also in the case of AP205, the sample inhomogeneity influences amide ^{1}H more than ^{1}Hα resonances.

IV. Pulse Program Schemes

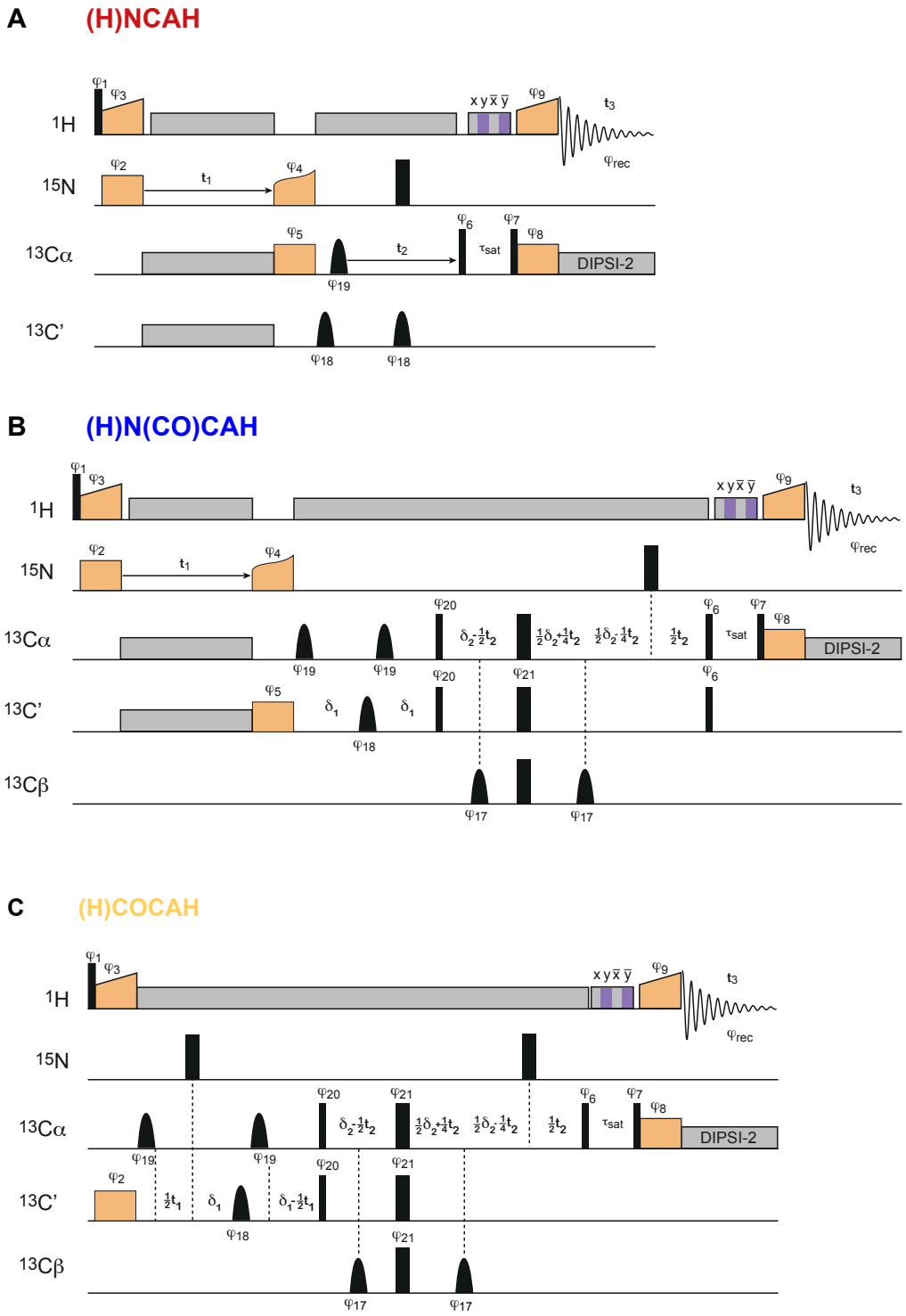

Figure S3. Pulse sequence schemes for (H)NCAH (A), (H)N(CO)CAH (B), (H)COCAH (C), (H)CO(N)CAH (D) and (HCA)CBCAH (E) experiments. Black narrow and wide boxes represent rectangular π/2 and π pulses, respectively. The "hard" pulse durations were 1.2 μs, 3.1 μs, 5.5 μs for ^{1}H, ^{13}C and ^{15}N, respectively. Bell-shaped pulses denote either Q3[9] or Re-Burp[10] refocusing pulses of the following durations and peak r.f. field: 160 μs and 20.6 kHz (Cα and C' Q3 pulses in A-D and Cαβ pulses in E), 680 μs and 9.2 kHz (Cβ ReBurp pulses in B and C). Cβ pulses were applied off-resonance at the ^{13}C offset of 23 ppm using phase modulation, while C' and Cα Q3 pulses were applied either on-resonance, or 60 or 120 ppm off-resonance depending on the current carrier frequency. Cross-polarization (CP) coherence transfers are denoted

D (H)CO(N)CAH

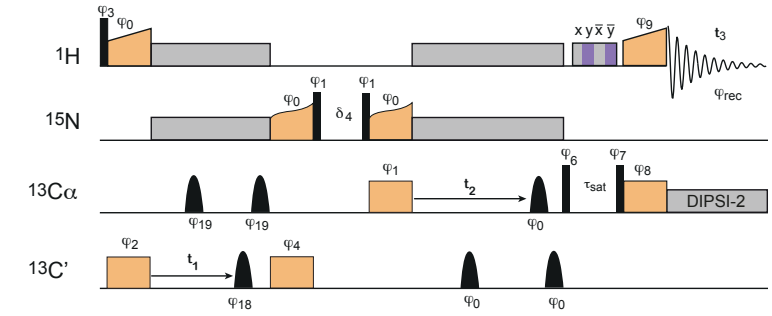

E (HCA)CBCAH

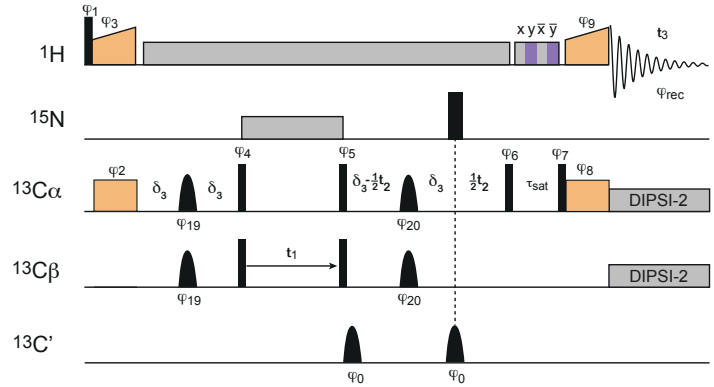

as orange rectangles and trapezes. Details of CP ramps, contact times and r.f. fields are summarized in the Supplementary Table S1. For GB1, the Cα-C' coherence transfer delays were set as follows $\delta_1 = 4.3$ ms, $\delta_2 = 4.0$ ms – pw_{ReBURP}. For AP205CP and HET-s, these delays were decreased to $\delta_1 = 3.9$ ms, $\delta_2 = 3.5$ ms – pw_{ReBURP}, $\delta_3 = 5.4$ ms to account for faster transverse dephasing. In (D), the z-filter time was $\delta_4 = 5$ ms. ^{1}H offset was set on resonance with H_2O resonance. ^{15}N offset was set to 117.8 ppm. In (A), ^{13}C carrier was placed in the center of ^{13}Cα resonances (56 ppm). In (B) and (C), the ^{13}C offset was kept in between of ^{13}Cα and ^{13}C' bands (116 ppm), and ^{13}C peaks folded by an integer multiple of respective spectral windows. In (D), the ^{13}C carrier frequency was changed from the centre of ^{13}C' (176 ppm) to ^{13}Cα resonances (56 ppm) during the delay δ_4. In (E), the ^{13}C offset was in the center of ^{13}Cβ (40 ppm) throughout the entire sequence, and the ^{13}Cα peaks were moved upfield in ω_2 by 16 ppm (equal to $sw_2/2$) by a phase decrementation of φ_6 by π every t_2 increment. MISSISIPI[11] with duration τ_{sat} of 100 ms and r.f. field $\gamma B_1/2\pi = 48.7$ kHz was used for suppression of water ^{1}H resonance. Grey rectangles represent homo- and heteronuclear composite pulse decoupling during frequency encoding (t_1-t_3) and *J*-based coherence transfers. Swept-TTPM ^{1}H decoupling[12] with r.f. field of 23.3 kHz and pulse width of 10 μs was employed. WALTZ-16[13] of 10 kHz r.f. and 25 μs pulse was applied for ^{15}N spins, and DIPSI-2[14] with 20 kHz r.f. and 12.5 μs pulse was used for ^{13}C decoupling. Pulse phases are as follows: $\varphi_1 = 2(y), 2(-y)$; $\varphi_2 = y$; $\varphi_3 = x$; $\varphi_4 = y$; $\varphi_5 = x$; $\varphi_6 = y$; $\varphi_7 = x$; $\varphi_8 = y$; $\varphi_9 = x$; $\varphi_{18} = x$; $\varphi_{19} = x, y$; $\varphi_{REC} = y, -y, -y, y$ (A); $\varphi_1 = 4(y), 4(-y)$; $\varphi_2 = 2(y), 2(-y)$; $\varphi_3 = x$; $\varphi_4 = y$; $\varphi_5 = x$; $\varphi_6 = y$; $\varphi_7 = x$; $\varphi_8 = y$; $\varphi_9 = x$; $\varphi_{17} = y$; $\varphi_{18} = y$; $\varphi_{19} = y$; $\varphi_{20} = x$; $\varphi_{21} = x, y$; $\varphi_{REC} = y, -y, -y, y, -y, y, y, -y$ (B); $\varphi_1 = 4(y), 4(-y)$; $\varphi_2 = 2(y), 2(-y)$; $\varphi_3 = x$; $\varphi_6 = y$; $\varphi_7 = x$; $\varphi_8 = y$; $\varphi_9 = x$; $\varphi_{17} = x$; $\varphi_{18} = x$; $\varphi_{19} = x$; $\varphi_{20} = y$; $\varphi_{21} = x, y$; $\varphi_{REC} = y, -y, -y, y, -y, y, y, -y$ (C); $\varphi_0 = x$; $\varphi_1 = y$; $\varphi_2 = 4(y), 4(-y)$; $\varphi_3 = 2(y), 2(-y)$; $\varphi_4 = y$; $\varphi_6 = x, -x$; $\varphi_7 = x$; $\varphi_8 = y$; $\varphi_9 = x$; $\varphi_{18} = x$; $\varphi_{19} = x$; $\varphi_{REC} = y, -y, -y, y, -y, y, y, -y$ (D); $\varphi_1 = y$; $\varphi_2 = 4(y), 4(-y)$; $\varphi_3 = 2(y), 2(-y)$; $\varphi_3 = x$; $\varphi_4 = y$; $\varphi_5 = y$; $\varphi_6 = x$; $\varphi_7 = x$; $\varphi_8 = y$; $\varphi_9 = x$; $\varphi_{19} = x$; $\varphi_{20} = x, y$; $\varphi_{REC} = y, -y, -y, y, -y, y, y, -y$ (E). Quadrature detection in ω_1 and ω_2 was accomplished using States-TPPI procedure[15] by incrementing φ_2 and decrementing φ_6 (A, B, C), or incrementing both φ_2 and φ_6 (D), or decrementing φ_2, φ_4 (jointly in t_1), and φ_6 (E) simultaneously with t_1 and t_2 time incrementation. All experiments were acquired at the ^{1}H B_0 field corresponding to ω_{0H} = 1000 MHz and MAS rate of $\omega_R = 100$ kHz.

For ^{13}Cα–^{13}C' transfers we suppress the undesired evolution of ^{13}Cα–^{13}Cβ couplings, and whenever possible, we utilize the coherence transfer delays δ_1 (in (C)), δ_2 (in (B,C)) and δ_3 (in (E)) for shared-time evolution to increase sensitivity and resolution in ^{13}C dimensions. Low-power decoupling was applied on the ^{1}H channel using the sw-TPPM (Swept Two-Pulse Phase Modulated) scheme[16], ensuring sample integrity during measurements.

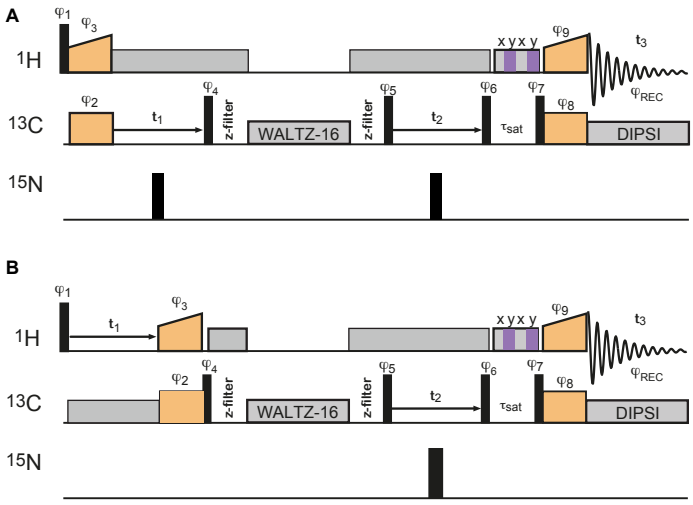

Figure S4. Pulse sequence schemes for (H)CCH-TOCSY (A), and H(C)CH-TOCSY (B). The same conventions and experimental settings are used as for Fig. S3. The ^{13}C carrier was placed in the center of aliphatic ^{13}C resonances (40 ppm). The following phase cycle was employed for both (A) and (B): $\varphi_1 = 2(y), 2(-y)$; $\varphi_2 = x, -x$; $\varphi_3 = x$; $\varphi_4 = y$; $\varphi_5 = 4(x), 4(-x)$; $\varphi_6 = -x$; $\varphi_7 = y$; $\varphi_8 = x$; $\varphi_9 = x$; $\varphi_{REC} = x, -x, -x, x$. WALTZ-16 decoupling[13] with $\gamma B_1/2\pi$ = 25 kHz or 27.7 kHz (i.e. a quarter of MAS rate) was employed for mixing of ^{13}C spins. Quadrature detection in ω_1 and ω_2 was accomplished using States-TPPI procedure[15] by incrementing φ_1 and φ_5 simultaneously with t_1 and t_2 time incrementation.

Table S1. Details of cross-polarisation transfers used in the experiments A-E in Fig. S1

CP transfer	Contact time	max. RF field, kHz		Pulse shape	
		Nucleus 1	Nucleus 2	Nucleus 1	Nucleus 2
^{1}H→^{13}C'	3000 μs$^{\$}$, 1000 μs$^{\#}$	134	33.4	Lin. ramp up 10%	Rectangle
^{1}H→^{13}Cα	400 μs$^{\#}$	134	28.8	Lin. ramp up 10%	Rectangle
^{1}H→^{15}N	1300 μs$^{\$}$, 1000 μs$^{\#}$	134	32.6	Lin. ramp up 10%	Rectangle
^{13}Cα→^{1}H	280 μs$^{\$}$, 300 μs$^{\#}$	41.7	134	Rectangle	Lin. ramp down 10%
^{13}C'→^{15}N	11 ms$^{\$}$, 12 ms$^{\#}$	62.7	38.9	Rectangle	Tangent up ± 10%*
^{15}N→^{13}Cα	11 ms, 12 ms$^{\#}$	38.9	62.1	Tangent up ± 10%*	Rectangle
^{15}N→^{13}C'	11 ms, 12 ms$^{\#}$	38.9	62.7	Tangent up ± 10%*	Rectangle

$^{\$}$ contact time used for GB1 sample

$^{\#}$ contact time used for AP205CP sample

* Tangent amplitude modulation $A(x)=1 + 0.1 \tan[2\alpha(x-0.5)]/\tan(\alpha)$, where α=1.22 (70 deg) and x varies from 0 to 1

V. Pulse Program Efficiency

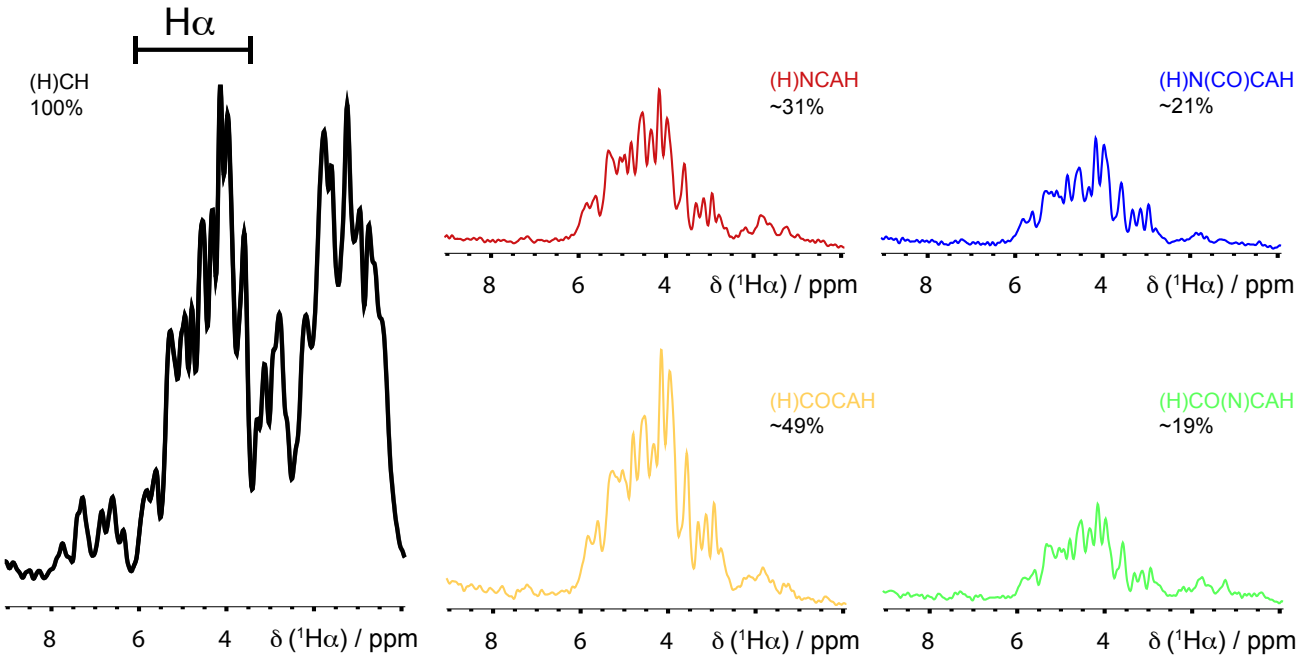

Figure S5. Relative sensitivity of four Hα-detected experiments, evaluated on a sample of GB1 at 100 kHz MAS. Fourier transform of the first increment is shown. 64 scans were added for each spectrum. Vertical scale as well as identical acquisition and processing parameters in the ^{1}H dimensions were applied. An approximate relative intensity (averaged) with respect to (H)CH is 0.31, 0.21, 0.49, and 0.19 for (H)NCAH, (H)N(CO)CAH, (H)COCAH and (H)CO(N)CAH, respectively.

VI. Acquisition And Processing Parameters

All spectra were recorded at $\omega_{0H}/2\pi$ =1 GHz and a MAS rate of 100 kHz (AP205CP, HET-s) or 111.111 kHz (GB1) using a Bruker 0.7 mm HCN probe.

Table S2. Acquisition and processing parameters for the NMR spectra of GB1. The direct proton dimension was sampled to 10 ms, and apodized with a 60-deg. shifted sine-bell squared. The spinning rate was 100 kHz, except the (H)CCH-TOCSY experiment where $\omega_R/2\pi$=111.111 kHz. The inter-scan delay was 1.0 s.

Spectrum	Max indirect evolution	Spectral window (ppm) [a]	Scans per point	Experimental time	Processing: window function (ω_1, ω_2)
(H)NCAH	13.8 ms (^{15}N) 6.5 ms (^{13}Cα)	32.9 (^{15}N) 30.0 (^{13}Cα)	4	11 h	60-deg shifted sine-bell squared
(H)N(CO)CAH	13.8 ms (^{15}N) 6.5 ms (^{13}Cα)	32.9 (^{15}N) 30.0 (^{13}Cα)	8	21.3 h	60-deg shifted sine-bell squared
(H)COCAH	6.5 ms (^{13}Cα) 7.4 ms (^{13}C')	30.0 (^{13}Cα) 15.0 (^{13}C')	4	7 h	60-deg shifted sine-bell squared
(H)CO(N)CAH	6.5 ms (^{13}Cα) 7.4 ms (^{13}C')	30.0 (^{13}Cα) 15.0 (^{13}C')	16	26 h	60-deg shifted sine-bell squared
(H)CCH TOCSY (15 ms)	6.8 ms (ω_1, ω_2)	66.0 (ω_1, ω_2)	2	32.5 h	90-deg shifted sine-bell squared

[a] 1 ppm ^{13}C = 251.5 Hz, 1 ppm ^{15}N = 101.4 Hz, 1 ppm ^{1}H = 1000 Hz

Table S3. Acquisition and processing parameters for the NMR spectra of AP205CP. The direct proton dimension was sampled to 10 ms, and apodized with a 90-deg. shifted sine-bell squared. The MAS rate was 100 kHz. The inter-scan delay was 1.2 s.

Spectrum	Max indirect evolution	Spectral window (ppm) [a]	Scans per point	Experimental time	Processing: window function (ω_1, ω_2)
(H)NCAH	9.86 ms (^{15}N) 6.36 ms (^{13}Cα)	40.0 (^{15}N) 30.0 (^{13}Cα)	2	6 h	90-deg shifted sine-bell squared
(H)N(CO)CAH	9.37 ms (^{15}N) 5.83 ms (^{13}Cα)	40.0 (^{15}N) 30.0 (^{13}Cα)	8	20.5 h	90-deg shifted sine-bell squared
(H)COCAH	5.3 ms (^{13}Cα) 6.3 ms (^{13}C')	30.0 (^{13}Cα) 15.0 (^{13}C')	4	6 h	90-deg shifted sine-bell squared
(H)CO(N)CAH	5.3 ms (^{13}Cα) 6.36 ms (^{13}C')	30.0 (^{13}Cα) 15.0 (^{13}C')	24	37.5 h	90-deg shifted sine-bell squared
(H)(CA)CBCAH	5.96 ms (^{13}Cα) 6.36 ms (^{13}C')	32.0 (^{13}Cα) 64.0 (^{13}Cβ)	4	17 h	60-deg shifted sine-bell squared
H(C)CH-TOCSY (15 ms)	2.86 ms (^{1}H) 4.54 ms (^{13}C)	14.0 (^{1}H) 70.0 (^{13}C)	4	23.5 h	90-deg shifted sine-bell squared
(H)CCH TOCSY (15 ms)	7.0 ms (ω_1, ω_2)	66.0 (ω_1, ω_2)	2	55 h	60/50-deg shifted sine-bell

[a] 1 ppm ^{13}C = 251.5 Hz, 1 ppm ^{15}N = 101.4 Hz, 1 ppm ^{1}H = 1000 Hz

Table S4. Acquisition and processing parameters for the NMR spectra of HET-S. The direct proton dimension was sampled to 5 ms, and apodized with a 60-deg. shifted sine-bell squared. The MAS rate was 100 kHz. The inter-scan delay was 1.0 s.

Spectrum	Max indirect evolution	Spectral window (ppm) [a]	Scans per point	Experimental time	Processing: window function (ω_1, ω_2)
(H)NCAH	7.15 ms (^{15}N) 3.98 ms (^{13}Cα)	40.0 (^{15}N) 30.0 (^{13}Cα)	12	14.5 h	60-deg shifted sine-bell squared
(H)N(CO)CAH	7.64 ms (^{15}N) 4.24 ms (^{13}Cα)	40.0 (^{15}N) 30.0 (^{13}Cα)	16	22 h	60-deg shifted sine-bell squared

[a] 1 ppm ^{13}C = 251.5 Hz, 1 ppm ^{15}N = 101.4 Hz, 1 ppm ^{1}H = 1000 Hz

VII. Completeness of Hα-detected Assignment Spectra

In the case of GB1 (56 a.a.), the acquired spectra showed all expected resonances in protein backbone. Considering that all 4 glycine residue show quite distinct ^{1}Hα shifts, the peak counts are: 60 for (H)NCAH and (H)COCAH, and 59 for (H)N(CO)CAH and (H)CO(N)CAH. Fig. S6 summarizes the signal-to-noise ratio of the observed peaks, normalized to a 24h acquisition time.

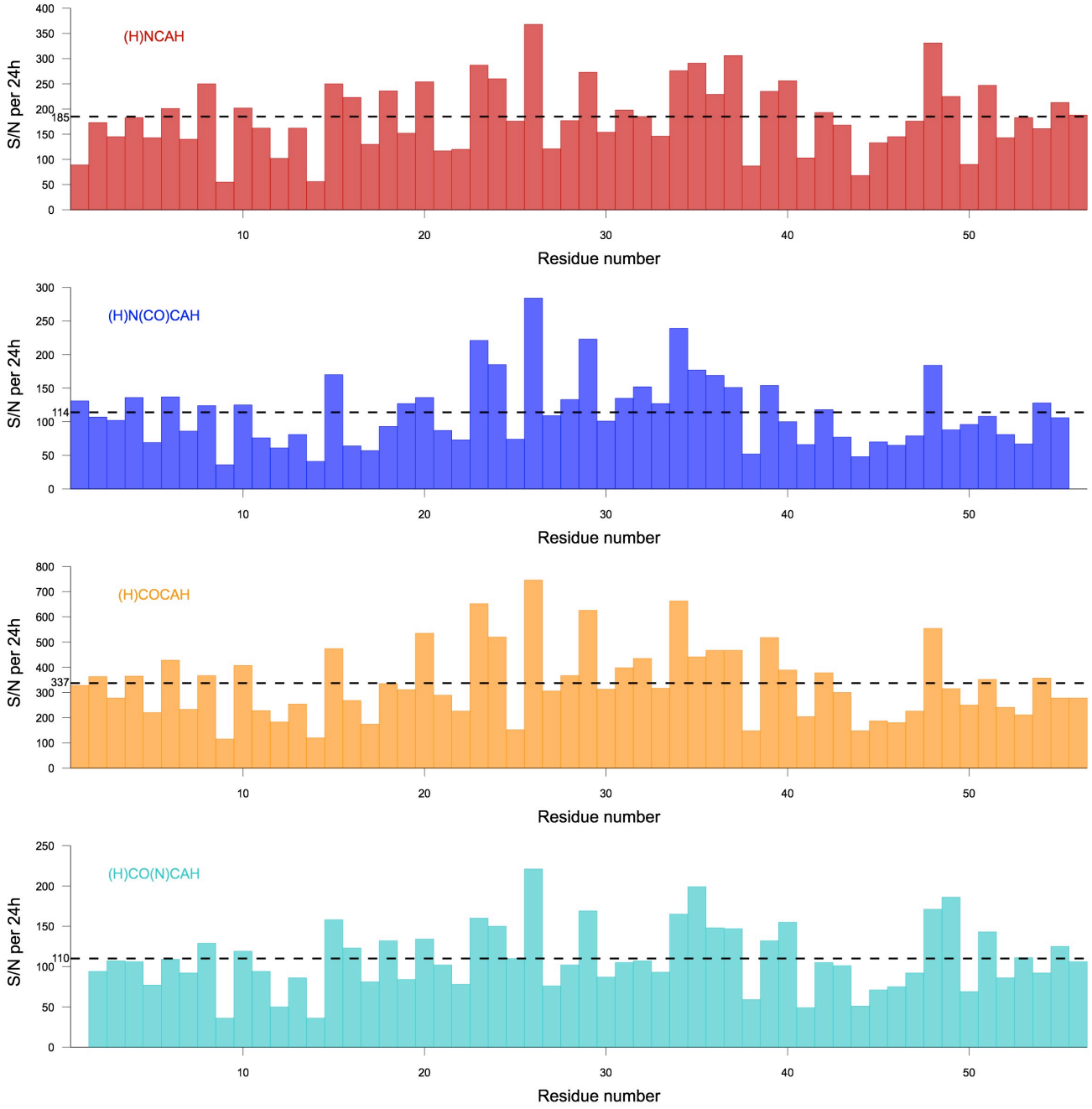

Figure S6. Signal to-noise-ratio for all peaks observed in (H)NCAH (top, in *brown*), (H)N(CO)CAH (second from the top, in *blue*), (H)COCAH (in *orange*) and (H)CO(N)CAH (bottom, in *cyan*) spectra recorded for GB1 sample. S/N was normalized to a 24 hour acquisition time by multiplying by a factor of $\sqrt{T_{24h}/T_{exp}}$. Average values are shown by dashed lines, and are in good agreement with sensitivity ratios observed for 1D acquisition (Fig. S5).

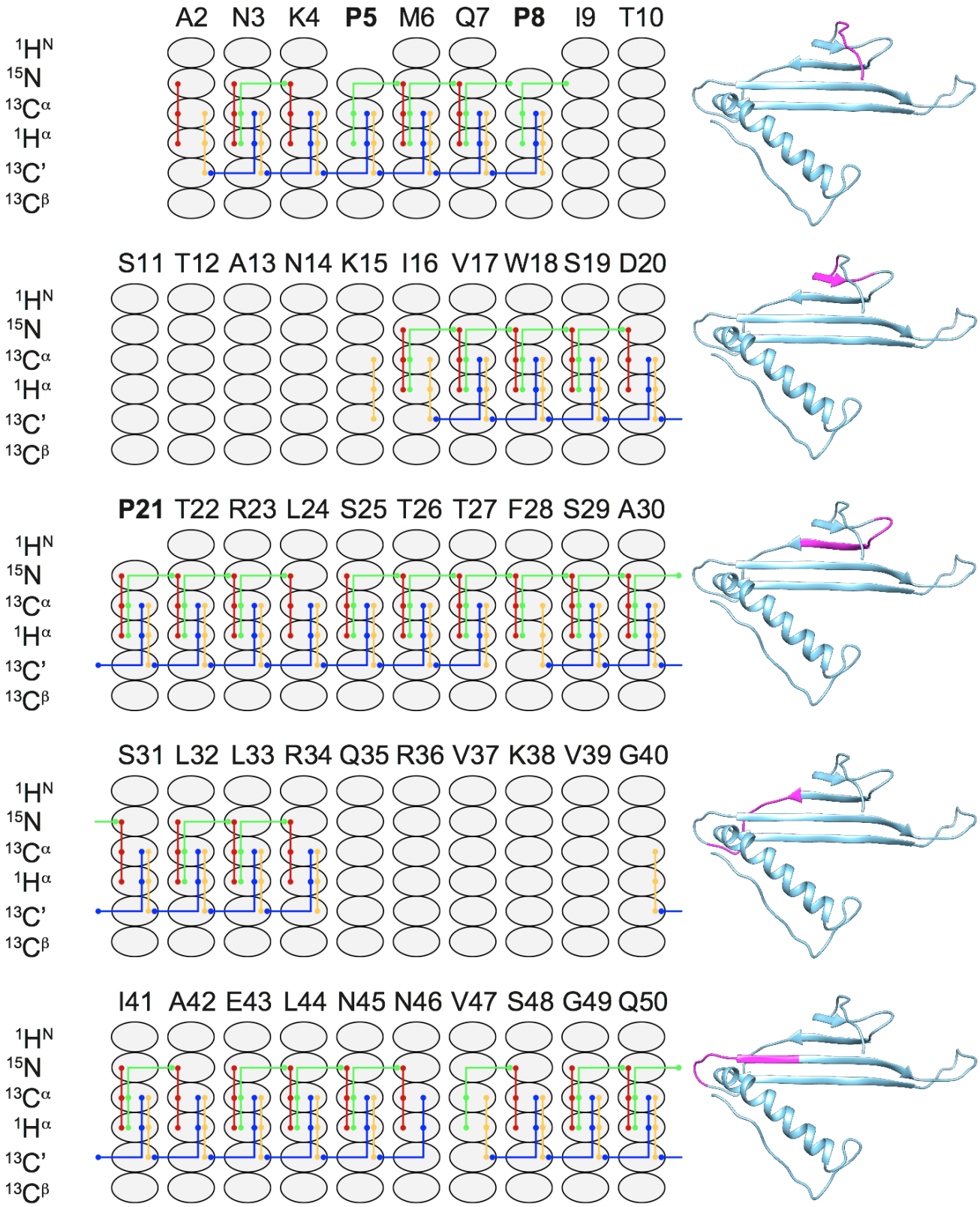

Figure S7. Sequential (*i*+1 and *i*-1) and intraresidual correlations observed in the three-dimensional experiments for AP205CP, shown as colored lines connecting respective resonances: (H)NCAH (in *brown*), (H)N(CO)CAH (in *green*), (H)COCAH (in *orange*), and (H)CO(N)CAH (in *blue*). Respective fragments of the protein sequence are highlighted in *pink* on the ssNMR structural model of the AP205 monomer.

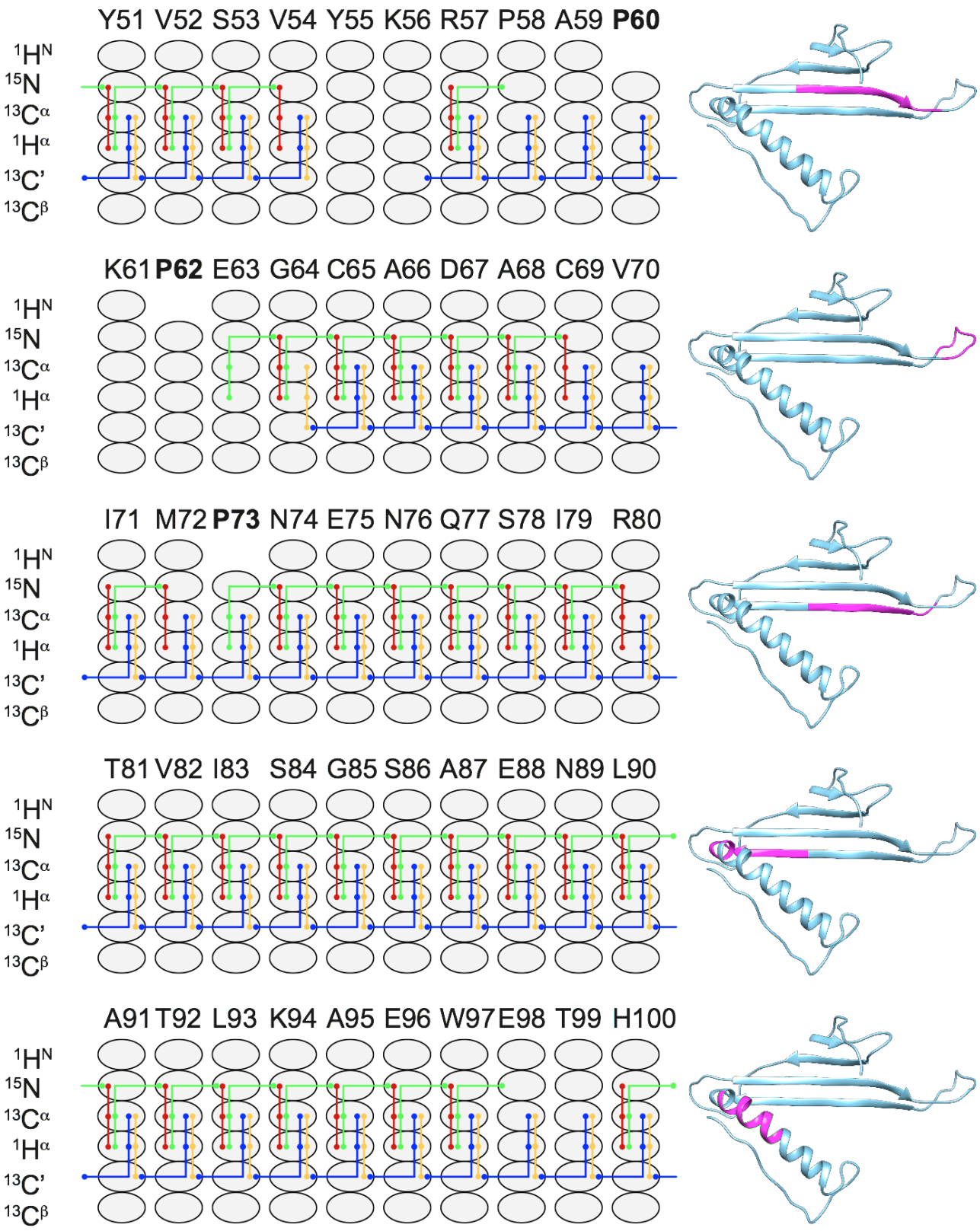

Figure S7. (continued).

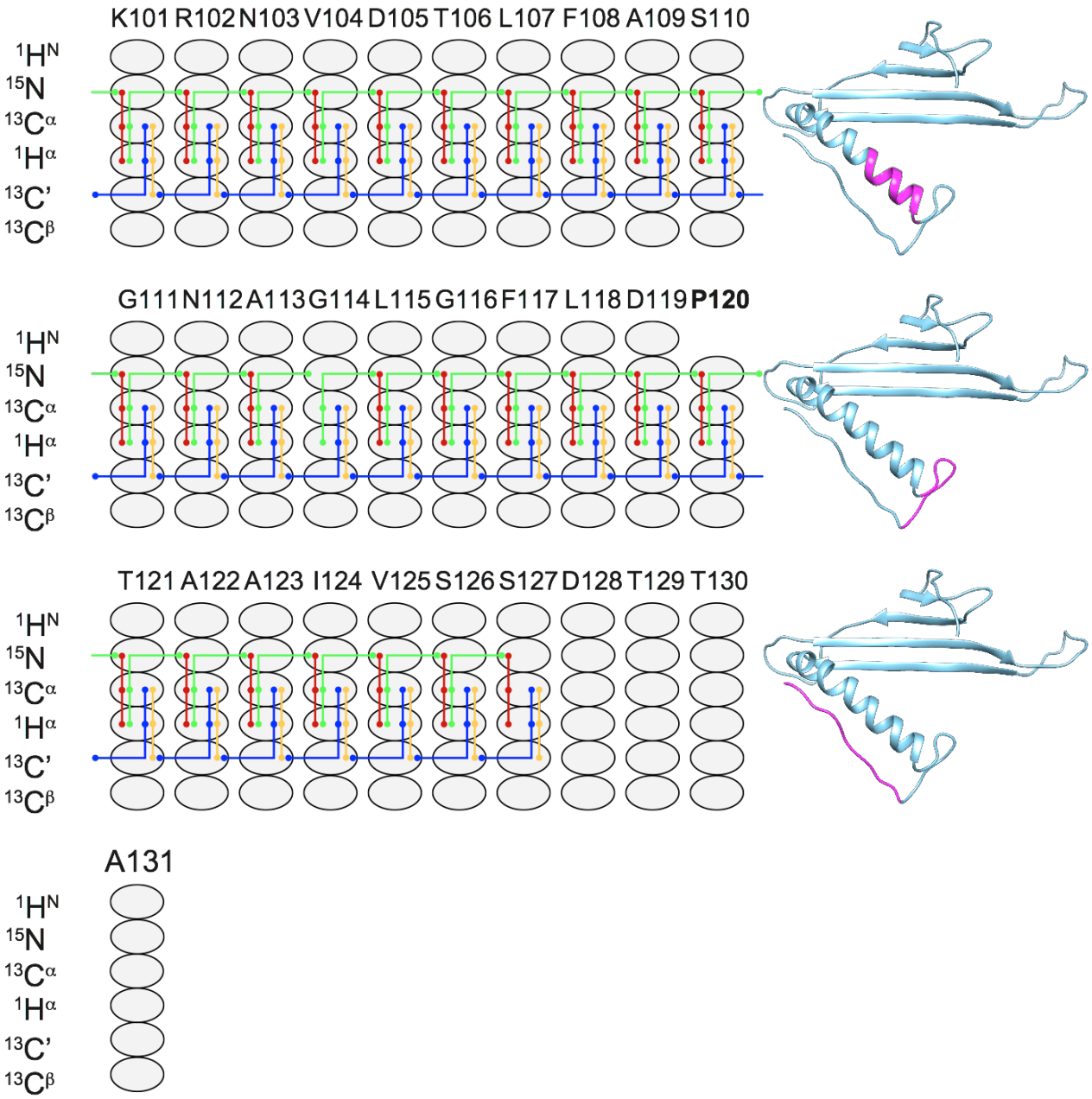

Figure S7. (continued).

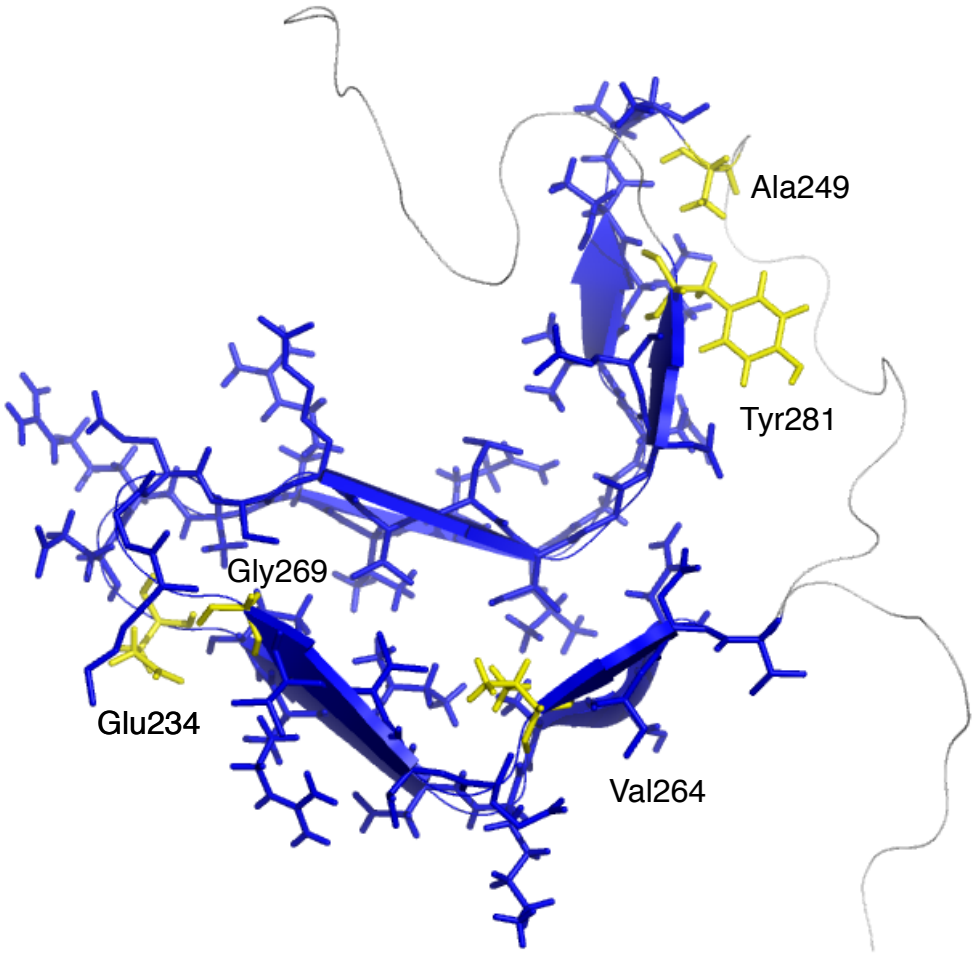

Figure S8. Summary of intra- and inter-residue correlations observed in the (H)NH, (H)CH, (H)NCAH and (H)N(CO)CAH spectra of HET-s(218-289) fibrils. Residues N226-A248 and T261-Y281 were considered as the rigid core of the amyloid fibrils, and thus represented by a stick model. Residues with missing assignments are labeled and colored in yellow. Glu 234 was not observed in the (H)NCAH spectrum, Ala 249 and Gly 269 did not show a correlation in the (H)NH spectrum, Val 264 could not been assigned due to chemical shift ambiguity, and Tyr 281 was not present in the (H)N(CO)CAH spectrum.

VIII. Proton Assignment of HET-s.

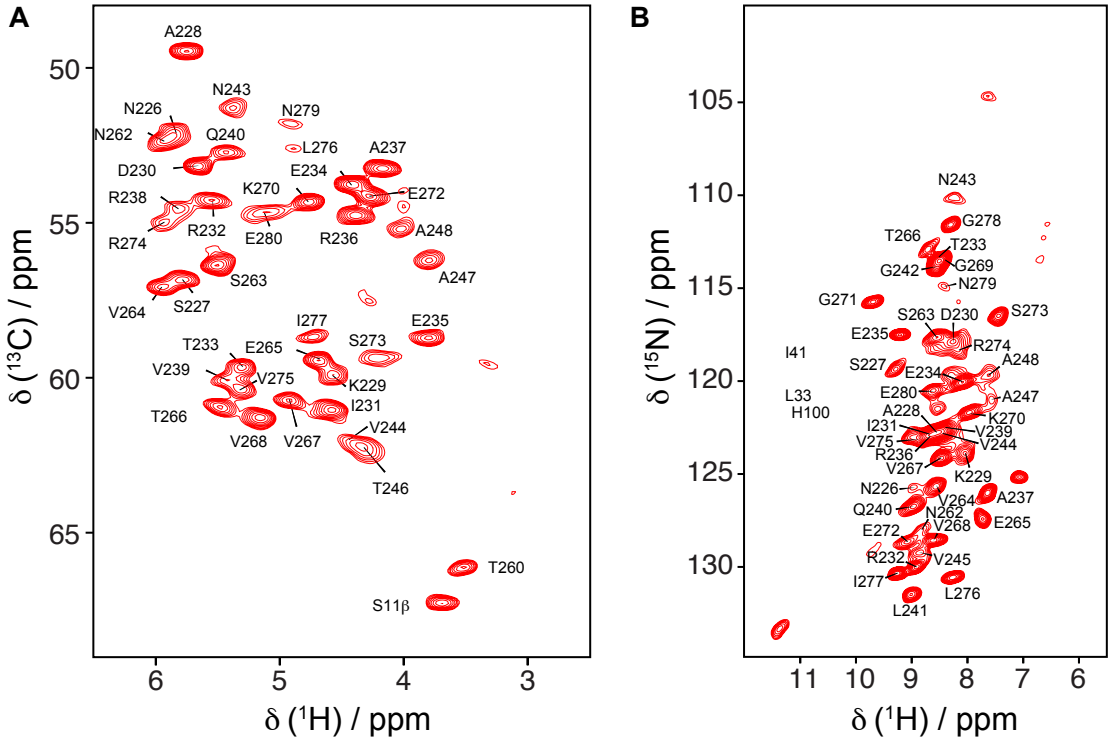

Figure S9. Assigned α-region of ^{13}C- (A) and ^{15}N-CP-HSQC (B) spectra of HET-s(218-289), recorded at 100 kHz MAS and on the 1 GHz spectrometer.

IX. Completeness of GB1 and AP205 Side-Chain Chemical Shifts

Only Hβ and Hγ resonances of Glu19 are missing among *aliphatic* protons in GB1. Effectively, the completeness of side-chain assignment of ^{1}H shifts is 99.1% (excluding hydroxyl, side-chain amine and amide as well as aromatic protons).

In the case of AP205CP, assignment of the ^{1}Hα and ^{13}Cα could not be obtained for the following 20 residues: Ile9-Lys15, Gln35-Val39, Lys56, Pro60-Pro62, Asp128-Ala131 (15% of residues). It was possible to assign 74.8% of side-chain ^{1}H protons (excluding hydroxyl, side-chain amine and amide as well as aromatic protons). If only residues with assigned ^{1}Hα and ^{13}Cα shifts are considered, the completeness of aliphatic side chain ^{1}H assignment is 87%.

Assigned chemical shifts were deposited in BioMagResBank under accession numbers 30088 (GB1) and 30094 (AP205CP).

X. References

1. W. T. Franks, D. H. Zhou, B. J. Wylie, B. G. Money, D. T. Graesser, H. L. Frericks, G. Sahota and C. M. Rienstra, *J. Am. Chem. Soc.*, 2005, **127**, 12291.
2. J. Klovins, G. P. Overbeek, S. H. E. van den Worm, H. W. Ackermann and J. van Duin, *J. Gen. Virol.*, 2002, **83**, 1523.
3. I. Bertini, F. Engelke, L. Gonnelli, B. Knott, C. Luchinat, D. Osen and E. Ravera, *J. Biomol. NMR*, 2012, **54**, 123.
4. A. Böckmann, C. Gardiennet, R. Verel, A. Hunkeler, A. Loquet, G. Pintacuda, L. Emsley, B. H. Meier and A. Lesage, *J. Biomol. NMR*, 2009, **45**, 319.
5. C. Wasmer, A. Lange, H. Van Melckebeke, A. B. Siemer, R. Riek and B. H. Meier, *Science*, 2008, **319**, 1523.
6. R. Spadaccini, O. Crescenzi, T. Tancredi, N. De Casamassimi, G. Saviano, R. Scognamiglio, A. Di Donato and P. A. Temussi, *J. Mol. Biol.*, 2001, **305**.
7. S. Leone, F. Sannino, M. L. Tutino, E. Parrilli and D. Picone, *Microb Cell Fact*, 2015, **14**.
8. A. J. Oakley, P. Prosselkov, G. Wijffels, J. L. Beck, M. C. Wilce and N. E. Dixon, *Acta Crystallogr D*, 2003, **59**.
9. L. Emsley and G. Bodenhausen, *J. Magn. Reson.*, 1992, **97**, 135.
10. H. Geen and R. Freeman, *J. Magn. Reson.*, 1991, **93**, 93.
11. D. H. Zhou and C. M. Rienstra, *J. Magn. Reson.*, 2008, **192**, 167.
12. A. E. Bennett, C. M. Rienstra, M. Auger, K. V. Lakshmi and R. G. Griffin, *J. Chem. Phys.*, 1995, **103**, 6951.
13. A. J. Shaka, J. Keeler, T. Frenkiel and R. Freeman, *J. Magn. Reson.*, 1983, **52**, 335.
14. A. J. Shaka, C. J. Lee and A. Pines, *J. Magn. Reson.*, 1988, **77**, 274.
15. D. J. States, R. A. Haberkorn and D. J. Ruben, *J. Magn. Reson.*, 1982, **48**, 286.
16. J. R. Lewandowski, J. Sein, H. J. Sass, S. Grzesiek, M. Blackledge and L. Emsley, *J. Am. Chem. Soc.*, 2010, **132**, 8252.